Superlattices and Microstructures 149 (2021) 106771

Contents lists available at ScienceDirect

Superlattices and Microstructures

journal homepage: www.elsevier.com/locate/superlattices

A DFT study on optoelectronic properties of near-infrared $In_{0.53}Ga_{0.47}As$ (001), (011) and (111) surfaces

Qianglong Fang [a], Yang Shen [a,*], Zesen Liu [b], Xiaodong Yang [c], Shuqin Zhang [a], Liang Chen [a,**], Lingze Duan [d], Shiqing Xu [a]

[a] Institute of Optoelectronics Technology, China Jiliang University, Hangzhou, 310018, China
[b] School of Electronic Science and Engineering, Nanjing University, Nanjing, 210023, China
[c] Key Laboratory of Ecophysics and Department of Physics, Shihezi University, Xinjiang, 832003, China
[d] Department of Physics, The University of Alabama in Huntsville, Huntsville, AL, 35899, USA

ARTICLE INFO

Keywords:
$In_{0.53}Ga_{0.47}As$ surfaces
First-principles
Surface energy
Work function
Optical properties

ABSTRACT

The III-V $In_xGa_{1-x}As$ photocathodes have important application prospects in the fields of marine submarine exploration, marine communication, and undersea imaging. Different semiconductor surfaces show different atomic arrangements, leading to different properties. In this paper, the optoelectronic properties of three representative $In_{0.53}Ga_{0.47}As$ surfaces have been studied and analyzed at the atomic levels by using the first-principles calculation method. Results show that the (001), (011) and (111) $In_{0.53}Ga_{0.47}As$ surfaces are all chemically stable, and the lowest work function is obtained at (001) surface. The band diagram shows that the conduction bands of the three surfaces are all shifted down to the Fermi level. At the same time, the valence bands on the (001) and (111) surfaces move up, crossing the Fermi level, indicating the enhancement of metallic property. The narrowing of the conduction band leads to the weakening of electron locality. Among the three representative surfaces, the average absorption coefficient and reflectance of $In_{0.53}Ga_{0.47}As$ (001) surface are decreased most significantly, reflecting higher photoelectrons emitting performance.

1. Introduction

The negative electron affinity (NEA) GaAs photocathodes own many advantages such as superior transmission characteristics, concentrated electron energy, angular distribution and so on. Therefore, it has become the focus of research in the fields of optoelectronic emission once it appears, and it has been widely used not only in low-light night vision imaging devices but also in particle physics fields such as electron beam exposure in a plane, design and application of linear accelerator [1–5]. The experiments by Turnbull and Evans as early as 1968 [6] demonstrated that the adsorption of alkali metal elements on the surface of GaAs photocathode can gain NEA properties. However, the limited spectral response threshold of GaAs photocathodes will further hinder its applications in ultraviolet and infrared regions [7,8]. With the participation of indium (In), the spectral response of $In_xGa_{1-x}As$ photocathode can be extended to the infrared region [9]. Moreover, the proportion of In component also affects the hybridization of electronic states and the material properties of crystal orientation [10]. A high quality $In_xGa_{1-x}As$ photodiode layer can be grown on the GaAs substrate,

* Corresponding author.
** Corresponding author.
E-mail addresses: yshen1016@foxmail.com (Y. Shen), lchen@cjlu.edu.cn (L. Chen).

https://doi.org/10.1016/j.spmi.2020.106771
Received 18 October 2020; Received in revised form 23 November 2020; Accepted 27 November 2020
Available online 30 November 2020

resulting in low dark current and high growth speed [11]. Furthermore, by depositing a strain buffer layer in the $In_xGa_{1-x}As$ heteroepitaxial layer on the GaAs substrate, the electrical activity of the defects can be extended [12]. When the component of x in $In_xGa_{1-x}As$ changes from 1 to 0, the energy bandgap will also change from 0.35 eV ($x = 1$) to 1.43 eV ($x = 0$), and accordingly, the cutoff wavelength varies from 3.5 μm to 0.87 μm [13]. In addition, previous researches have proposed that the emission layer of $In_xGa_{1-x}As$ photocathode matches the substrate well and the lattice mismatch is the smallest when $x = 0.53$ [14,15], which is helpful for the formation of NEA $In_xGa_{1-x}As$ photocathodes.

Semiconductor materials have different atomic arrangements along the surface in different directions, which will lead to different surface characteristics. In this study, the atomic structure and optoelectronic properties of $In_{0.53}Ga_{0.47}As$ (001), (011), and (111) surfaces are simulated and analyzed. The surface energies, work functions, E-Mulliken populations, band structures, density of states and optical characteristics of three representative $In_{0.53}Ga_{0.47}As$ surfaces are calculated. The accurate calculation and quantitative analysis will contribute to the design of high-performance NEA $In_{0.53}Ga_{0.47}As$ photocathodes.

2. Calculation method and models

The calculation used in this article adopts the Perdew−Burke−Ernzehof (PBE) functional in view of the density functional theory (DFT) [16,17], and the program package *Cambridge Serial Total Energy Package* (CASTEP) [18–20] is selected for the calculation. As is known, the hybrid exchange correlation functionals, like B3LYP or B3PW, allows to achieve an excellent agreement with the experiment for the band gaps of related complex materials [21,22], whereas the DFT based PBE usually underestimates the band gap of those complex materials. However, it does not influence the analysis of the electronic properties of the calculated structures [23,24]. Meanwhile, the Broyden-Fletcher-Goldfarb-Shanno (BFGS) [25] arithmetic is selected to obtain the optimized bulk material constructions. A self-consistent method is also adopted to perform dipole correction to reduce the impact of dipole moment. The calculations are performed using the valence electronic states of the constituting atoms as following: In:$4d^{10}5s^25p^2$, Ga:$3d^{10}4s^24p^1$, As:$4s^24p^3$, H:$1s^1$. Based on the principle of minimum energy, the convergence accuracy of energy and force are set to 2×10^{-6} eV/atom and 0.002 eV/nm, respectively. The upper limit of convergence for a single atom is 2×10^{-5} eV, working tension smaller than 0.03 GPa, and the offset of the atom changes less than 0.0001 nm during the iteration. In order to prevent the interactions between adjacent plates, the thickness of the vacuum layer is selected to 15 Å. After multiple convergence tests, the best truncation energy is selected as 400 eV, the k grid points for $In_{0.53}Ga_{0.47}As$ bulk material and the three surfaces are selected as $7 \times 7 \times 7$ and $4 \times 6 \times 1$, respectively, and the calculation of optical properties is corrected by the scissor's operator [26].

The $In_{0.53}Ga_{0.47}As$ primitive cell crystal model is shown in Fig. 1. Fig. 2 depicts the top and side views of the optimized slab models of (001), (011) and (111) $In_{0.53}Ga_{0.47}As$ surfaces. As can be seen from Fig. 2, there are 56 atoms in the $In_{0.53}Ga_{0.47}As$ (001) and (111) surface models: 13 In atoms, 11 Ga atoms, 28 As atoms, and 4 extra pseudo hydrogen atoms. However, there are 64 atoms on the surface of (011) model: 15 In atoms, 13 Ga atoms, 28 As atoms, and 8 extra pseudo hydrogen atoms. Therefore, the stoichiometric ratio of In atoms in the three surfaces of $In_{0.53}Ga_{0.47}As$ all agrees well with $x = 0.53$. The atomic arrangements of the three surfaces consist of seven bilayers of atoms. In order to simulate a large environment to improve the calculation accuracy, the three bimolecular layers at the top of the model are freely relaxed, while the four bimolecular layers at the bottom of the model are fixed. Meanwhile, the bottom of the model is equipped with pseudo-hydrogen atoms to avoid the metastasis of electrons on the surface [27].

3. Calculation results and analysis

3.1. Surface energy

Surface energy is often used to judge the stability of the atomic structures, and can be quantitatively described by σ, which can be optimized by the following expression [28–30]:

$$\sigma A = \left(E_{slab}^{tot} - N_{Ga}\mu_{Ga} - N_{In}\mu_{In} - N_{As}\mu_{As} - N_H\mu_H\right) \quad (1)$$

where *Etot slab* is the total energy of the plate model, N_i is the amount of type i atoms in the model, μ_i is the energy of an i-type atom. A is the total surface area, μ_{Ga}, μ_{In}, and μ_{As} are independent of each other and satisfy the following formula: $0.47\mu_{Ga} + 0.53\mu_{In} + \mu_{As} = E_{bulk}$,

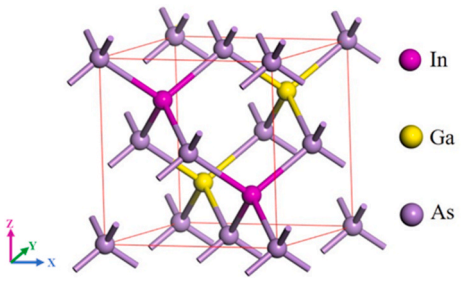

Fig. 1. $In_{0.53}Ga_{0.47}As$ primitive cell crystal model.

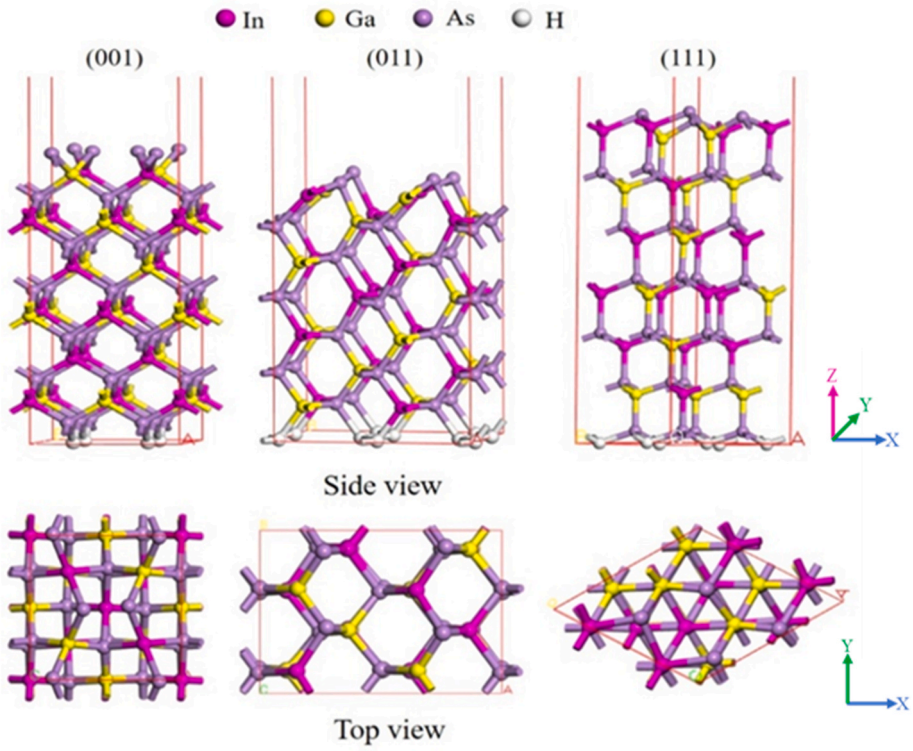

Fig. 2. Top and side views of (001), (011) and (111) $In_{0.53}Ga_{0.47}As$ surfaces, respectively.

so we can get the following formula:

$$\sigma A = \left(E_{slab}^{tot} - \frac{N_{Ga}(E_{bulk} - \mu_{As} - 0.53u_{In})}{0.47} - N_{In}\mu_{In} - N_{As}\mu_{As} - N_H\mu_H \right) \tag{2}$$

where E_{bulk} represents the average energy of $In_{0.53}Ga_{0.47}As$ bulk model. Here we define $0.53N_{Ga}/0.47$ as δ. For (001) and (111) surfaces, the value of δ is about 12.404, and for (011) surface, the value of δ is about 14.659. When we approximate that δ and N_{In} are equal, we can get that σ can be written as a formula only related to As atoms:

$$\sigma A = \left(E_{slab}^{tot} - N_{Ga}(E_{bulk} - \mu_{As}) \right) / 0.47 - N_{As}\mu_{As} - N_H\mu_H \tag{3}$$

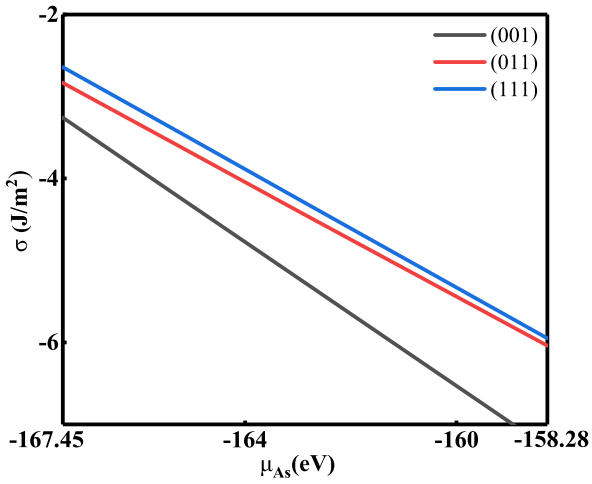

Fig. 3. Surface energies of $In_{0.53}Ga_{0.47}As$ bulk model and three representative surfaces.

The calculated surface energies of (001), (011) and (111) $In_{0.53}Ga_{0.47}As$ surfaces are shown in Fig. 3. Obviously, all three surfaces have negative surface energy, indicating the formation of the three surfaces is an exothermic process. The (001) surface is the most stable, while the (011) and especially the (111) surfaces are less stable. The same phenomenon also occurs in another materials, for example, ABO_3 perovskites [31].

3.2. Work function

In semiconductors, the work function, also known as escape work, refers to the minimum value of energy which an electron needed to escape into the vacuum, and the calculation formula is as follows [32]:

$$\phi = E_{vac} - E_f \tag{4}$$

where, E_{vac} represents the potential of the vacuum level and E_f represents the potential of the Fermi energy, respectively. The calculated work functions of the (001), (011), and (111) $In_{0.53}Ga_{0.47}As$ surfaces are 4.542eV, 4.743eV and 5.103eV, respectively. Obviously, according to the calculation result, the work function of (001) surface is the lowest, photoelectrons on (001) surface can escape into vacuum easier than that on (011) and (111) surfaces.

3.3. E-Mulliken population

The number of E-Mulliken bond and atomic populations of bulk, (001), (011) and (111) $In_{0.53}Ga_{0.47}As$ surfaces are calculated and shown in Table 1. By referring to the electronegativity table proposed early, the relative electronegativity of In, Ga and As atoms are 1.78, 1.81 and 2.18 [33], respectively, indicating that In–As bond and Ga–As bond are held together by the covalent interaction of atoms. As can be seen from Table 1, the bond populations of Ga–As and In–As are all increased, indicating the covalent properties are further enhanced. Obviously, the covalency of In–As bonds are greater than that of Ga–As bonds. The E-Mulliken atom populations show that Ga 3d and In 4d states remain basically unchanged, the electron number of Ga 4s state increases, while the numbers of Ga 4p, In 5s, In 5p, As 4s and As 4p electron state decrease, respectively. The redistribution of electron states leads to the breakdown of sp^3 hybridized orbital and the formation of plane sp^2 hybridized orbital. Moreover, the changes in the s and p states of Ga atom are more obvious than those of In and As atoms, indicating that the Ga–As bond varies more obvious during surface formation, which is consistent with the variation of bond population.

3.4. Band structure and density of states

The energy band diagrams of the bulk $In_{0.53}Ga_{0.47}As$ and three representative surfaces are shown in Fig. 4, in which the Fermi energy level is fixed at 0 eV. The band gap of bulk material is calculated as 0.382 eV, which is smaller than the band gap obtained by experiment (0.782eV). This is caused by the common choice of energy states, since the ground state is selected by the DFT, while the band gap is an excited state [34]. Obviously, the conduction band minimum (CBM) of all three surfaces shift downwards, while the valence band maximum (VBM) of (001) and (111) surfaces shift upwards, respectively. The movement of the electrons at the atomic orbitals contributes to the formation of surface state, which further resulting in band gap narrowing. In addition, the narrowing of the conduction band reflects the reduced electron effective mass at the CBM, and further results in the weakening of electronic locality. The enhancement of metallic characteristics is conducive to electron transport on the surface, leading to the enhancement of surface conductivity.

Fig. 5 shows the total and partial density states of $In_{0.53}Ga_{0.47}As$ bulk and three representative surfaces. Clearly, the peak at −14.8 eV is mainly caused by Ga 3d and In 4d states. The lower valence band at −13.4 ∼ −9.6 eV is mainly caused by As 4s, while the upper valence band at −7.7–0 eV is mainly caused by Ga 4s, In 5s, In 5p and As 4p states, respectively. For the conduction band of three surfaces, it mainly consists of In 5p, Ga 4p and As 4p states. In addition, in bulk $In_{0.53}Ga_{0.47}As$ and three representative (001), (011) and (111) surfaces, *p* electronic states associated with In and Ga atoms are positioned in the upper portion of the valence band, while In(Ga) *s* states are located in the lower portion of the band. This is also consistent with the results obtained from other mixed In-Ga-bearing semiconductors [35,36].

Table 1
E-Mulliken populations of bulk, (001), (011) and (111) $In_{0.53}Ga_{0.47}As$ surfaces.

		Bulk	(001)	(011)	(111)
bond population	Ga–As	−1.62	0.31	0.42	0.48
	In–As	0.65	0.79	0.73	0.92
Ga atom population	4s	0.62	1.02	1.12	1.03
	4p	1.76	1.69	1.65	1.71
	3d	9.99	10.0	10.0	10.0
In atom population	5s	1.47	1.37	1.36	1.35
	5p	1.64	1.58	1.53	1.58
	4d	9.98	9.99	9.99	9.99
As atom population	4s	1.62	1.56	1.51	1.57
	4p	3.64	3.58	3.63	3.56

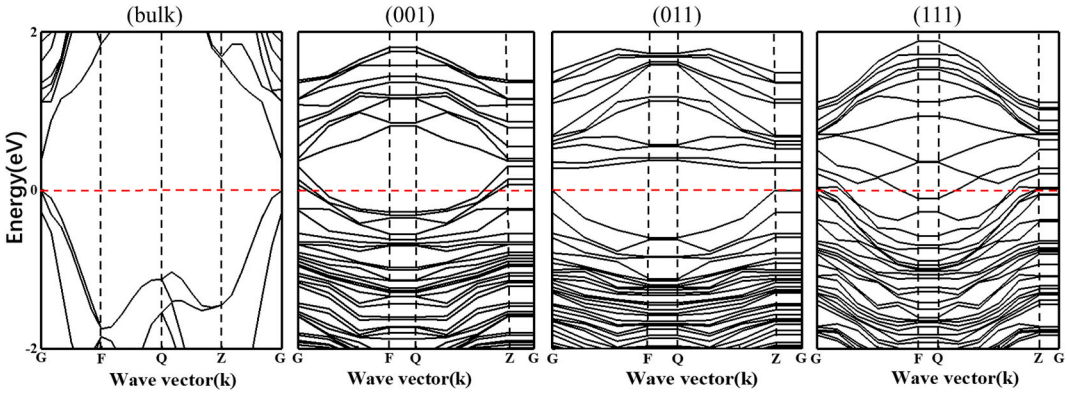

Fig. 4. The band structures of $In_{0.53}Ga_{0.47}As$ bulk model and three representative surfaces.

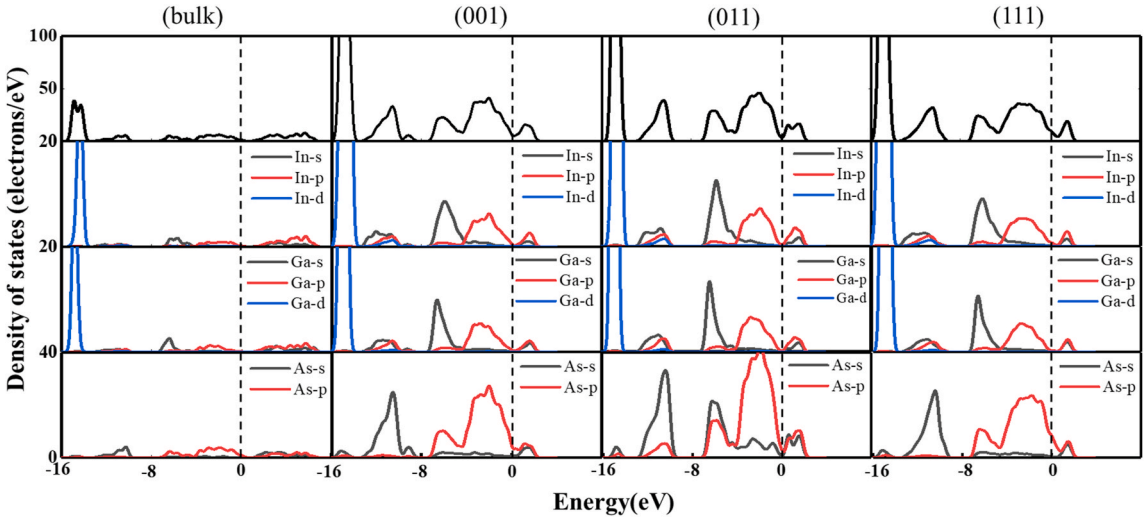

Fig. 5. The total and partial density states of $In_{0.53}Ga_{0.47}As$ bulk and three representative surfaces.

3.5. Optical properties

For semiconductor materials, the optical response characteristics between solids in the near-infrared linear spectral response range can be described by the complex dielectric function $\varepsilon(\omega) = \varepsilon_1(\omega) + i\varepsilon_2(\omega)$ or by complex refractive index $N(\omega) = n(\omega) + ik(\omega)$ [37]:

$$\varepsilon_1 = n^2 - k^2 \tag{5}$$

$$\varepsilon_2 = 2nk \tag{6}$$

Adiabatic approximation assumes that the nucleus of an electron is stationary when it is moving, that is, the electronic motion is adiabatic to the nucleus. The one-electron approximation can ignore the participation of phonons in the band transition and only consider the excitation of the electrons. In addition, through the understanding and derivation of the direct transition probability and the Kramers-Kronig dispersion relation, the complex dielectric function, the absorption coefficients and reflectivity of the material can be obtained as follows [38,39]:

$$\varepsilon_2(\omega) = \frac{\pi}{\varepsilon_0}\left(\frac{e}{m\omega}\right)^2 \sum_{V,C}\left\{\int_{BZ}^{\infty} \frac{2dk}{(2\pi)^2}\left|aM_{V,C}\right|^2 \delta[E_C(K) - E_V(K) - h\omega]\right\} \tag{7}$$

$$\varepsilon_1(\omega) = 1 + \frac{2e}{\varepsilon_0 m^2}\sum_{V,C}\int_{BZ}^{\infty} \frac{2dk}{(2\pi)^2}\frac{\left|aM_{V,C}(K)\right|^2}{[E_C(K) - E_V(K)]/h}\frac{1}{[E_C(K) - E_V(K)]^2/h^2 - \omega^2} \tag{8}$$

$$\alpha = 2\omega k/c = 4\pi k/\lambda_0 \tag{9}$$

$$R(\omega) = \left[(n-1)^2 + k^2\right] / \left[(n+1)^2 + k^2\right] \tag{10}$$

In the above formulas, k is the extinction coefficient of the material, n is the complex refractive index parameter of the material, K represents the wave vector of plane wave, a represents the unit vector A, BZ represents the first Brillouin region in the reciprocal space, C represents the conduction band and V represents the valence band, $M_{V,C}$ is the element in the transformation matrix. $E_C(K)$ and $E_V(K)$ represent the CBM and the VBM energy levels of the intrinsic semiconductor, respectively.

The imaginary part of the complex dielectric constant is caused by various relaxation polarizations, which are associated with changes in the material's internal steering polarization and external high-frequency electric fields representing the material's loss term. In addition, the irradiation of light can cause the electron absorption energy to transition from the VBM to the CBM. Therefore, the complex dielectric constant material can be used to quantitatively describe the relationship between the photon energy absorbed per unit volume in unit time and the electromagnetic wave power.

The calculation results of the real and imaginary parts of the complex dielectric function of $In_{0.53}Ga_{0.47}As$ bulk and three surfaces are shown in Fig. 6. It is clearly seen that, compared with the bulk model, the (001) and (011) surfaces have smaller intersection values with the y-coordinate axis, that is, their static dielectric constants are smaller, while the parameter of the (111) surface is greater. In the figure, the first peak of the imaginary part of the volume material is 2.05eV, while the first peak of the imaginary part of the surface (001), (011) and (111) is 1.76eV, 1.23eV and 0.50eV, respectively. The peak of the imaginary part moves towards the direction of low energy, indicating the movement of electrons at the atomic orbitals.

Complex refractive index is the most important optical constant for absorbing media. The real part represents the refractive index of the medium, and the imaginary part represents the absorption coefficients, which can be used to describe the absorption characteristics of the medium and the polarization state of the reflected and transmitted light.

Fig. 7 depicts the complex refractive index of $In_{0.53}Ga_{0.47}As$ bulk, and three representative surfaces. When $\varepsilon_1 < 0$ ($n < k$), a strong inter-band transition occurs, and thus the material exhibits a strong metallic reflectivity. The metal reflection (MR) regions of the bulk and the other three surfaces are 4.28–15.1 eV, 2.13–6.33 eV, 2.68–5.41 eV, 2.63–5.65 eV, respectively. The MR regions of the three surfaces are smaller than that of the bulk material, and move towards a lower energy side. The MR region of the (011) surface is the smallest, while the (011) surface has the largest change. As is known, when the refractive index of a material increases with increasing incident photon frequency, the material exhibits normal dispersion. Otherwise, the material exhibits abnormal dispersion. Taking the (001) surface as an example, the material exhibits abnormal dispersion in the region of 0–6.34 eV, while in the region of 6.34–20 eV, the material exhibits normal dispersion.

The calculated optical absorption spectrum of $In_{0.53}Ga_{0.47}As$ bulk and three representative surfaces are shown in Fig. 8. The peaks of absorption coefficient of the $In_{0.53}Ga_{0.47}As$ bulk locate at 2.09 eV (contributes to the transition between As 4p, Ga 4p and In 5p state electrons), 4.75 eV (contributes to the transition of As 4p state electron), 6.71 eV (contributes to the transition of As 4p state electron), 8.97 eV (contributes to the transition between Ga 4s and In 5s state electrons),17.2 eV (contributes to the transition of As 4s state electron),19.9 eV (contributes to the transition between Ga 3d and In 4d state electrons). Compared with the bulk material, the peaks of the absorption coefficient on the surfaces are greatly reduced, and the band edges of the absorption spectra move towards a lower energy direction.

Fig. 9 shows the reflectivity spectrum of $In_{0.53}Ga_{0.47}As$ bulk and three surfaces. As can be seen from the figure, the average reflectance of the three surfaces is smaller when compared with the bulk, and the parameter of the (011) surface is the smallest. The reflectivity failing edge of the surfaces are all moving to a lower energy side. Meanwhile, the movement of (011) surface is the most obvious. The higher the reflection coefficient, the more difficult it is for electrons transporting to the surface. Therefore, in order to obtain better photoemission effect, the surface with low reflectance should be selected.

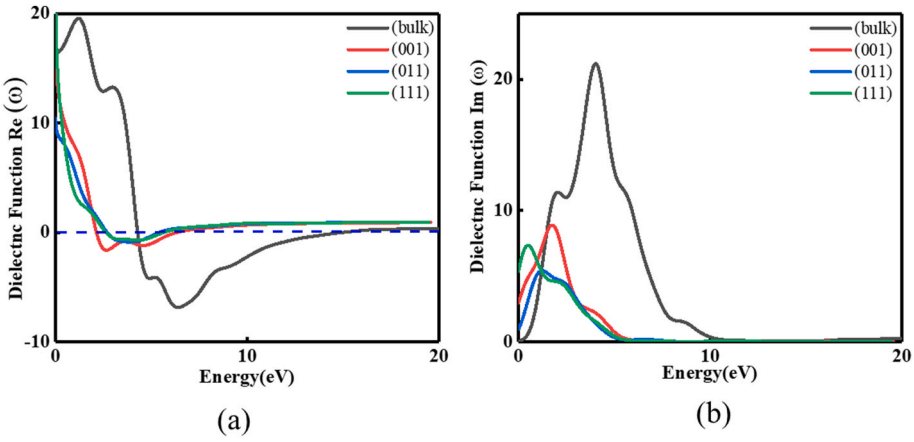

Fig. 6. The dielectric function of $In_{0.53}Ga_{0.47}As$ bulk and three surfaces, (a) real and (b) imaginary part, respectively.

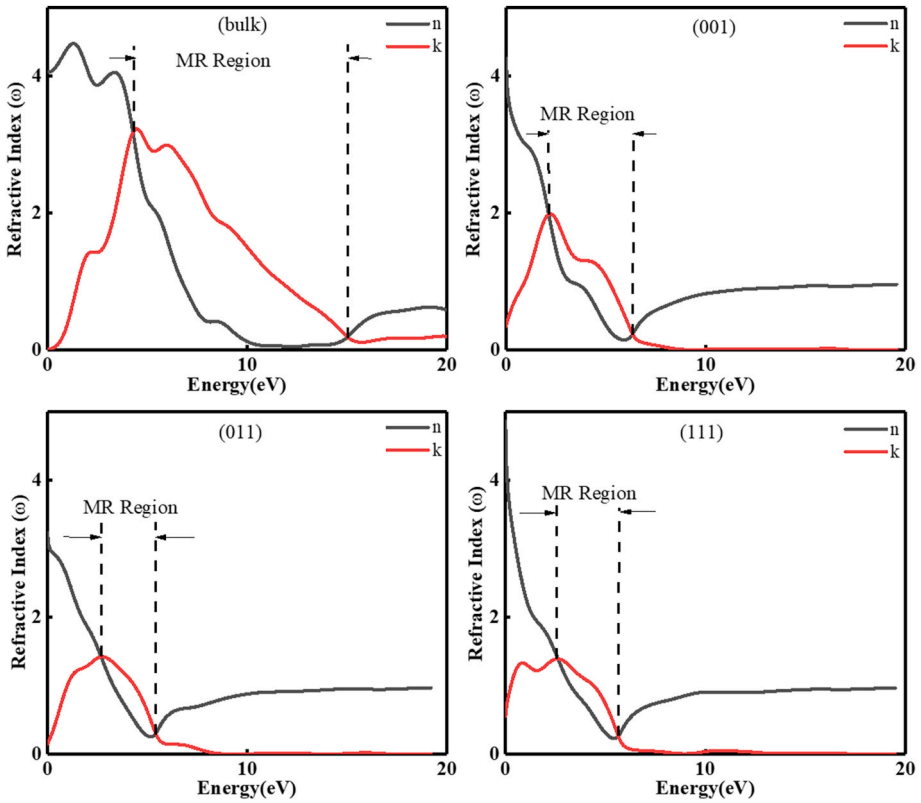

Fig. 7. The refractive Index of $In_{0.53}Ga_{0.47}As$ bulk model and three representative surfaces.

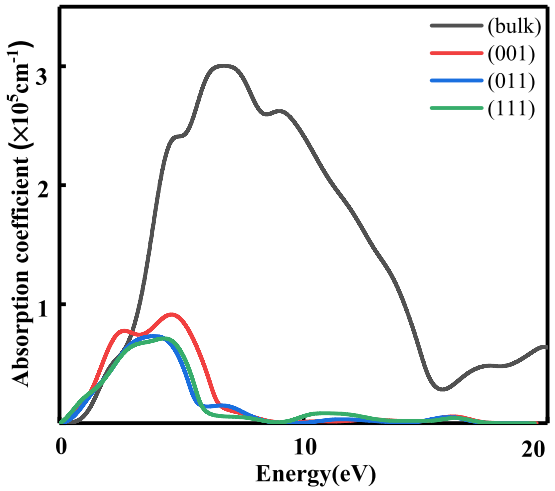

Fig. 8. The absorption spectrum of $In_{0.53}Ga_{0.47}As$ bulk model and three representative surfaces.

By comparing the emission and absorption curves, the absorption and reflection coefficients of (001) surface are the smallest, indicating the higher transmittance of (001) surface, which is conducive to photoelectrons emitting.

4. Conclusion

In summary, using CASTEP program package, the atomic and electronic structures and optical properties of $In_{0.53}Ga_{0.47}As$ (001), (011) and (111) surfaces are studied within DFT approach. Results show that the three representative surfaces of $In_{0.53}Ga_{0.47}As$ are all chemically stable. The $In_{0.53}Ga_{0.47}As$ (001) surface has smaller work function than the other two surfaces, reflecting the photons are

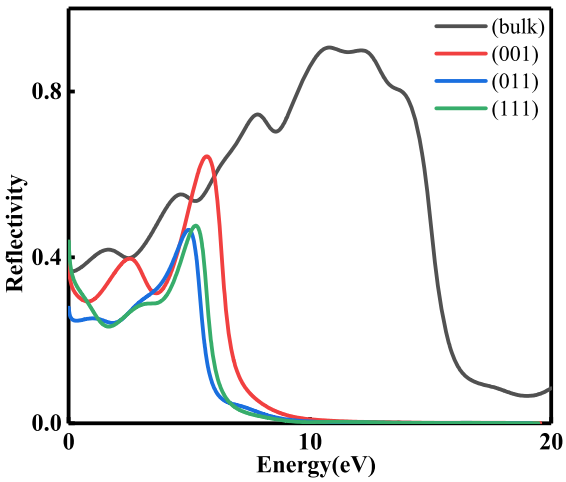

Fig. 9. Reflectivity spectrum of $In_{0.53}Ga_{0.47}As$ bulk model and three representative surfaces.

most likely to escape into the vacuum. The CBM of all three surfaces are shifted down to the Fermi level while the VBM of (001) and (111) surfaces tend to move up. The narrowing of the conduction band leads to the weakening of electron locality. The MR regions of all three surfaces are narrower than that of the bulk material, and move towards a lower energy direction. Although the MR regions of (011) $In_{0.53}Ga_{0.47}As$ surface is the narrowest, the change of the (001) surface is the largest. Compared with the bulk material, the absorption coefficients and reflectivity of all three surfaces are obviously smaller. Due to the smallest work function, average absorption coefficient and reflectivity, $In_{0.53}Ga_{0.47}As$ (001) surface has the strongest electron emitting performance among the three representative surfaces.

Credit author statement

Qianglong Fang: Investigation, Writing-Original Draft. **Yang Shen:** Conceptualization, Writing-Review & Editing, Supervision. **Zesen Liu:** Investigation, Resources. **Xiaodong Yang:** Software, Methodology. **Shuqin Zhang:** Validation, Investigation. **Liang Chen:** Resources, Formal analysis. **Lingze Duan:** Investigation, Visualization. **Shiqing Xu:** Resources, Project administration.

Declaration of competing interest

The authors declare that they have no known competing financial interests or personal relationships that could have appeared to influence the work reported in this paper.

Acknowledgement

This work was supported by the National Natural Science Foundation of China (Grant Nos. 61775203, 62004183 and 62075205), the National Key Research and Development Program of China (Grant No. 2017YFF0210800), Natural Science Foundation of Zhejiang Province (Grant Nos. LZ20F050001, LQ21F050011 and LGG19F050005) and the Fundamental Research Funds for the Provincial Universities of Zhejiang (Grant No. 2020YW48).

References

[1] G.A. Allen, J. Phys. D Appl. Phys. 4 (1971) 308–317.
[2] R. Alley, H. Aoyagi, J. Clendenin, Nucl. Instrum. Methods Phys. Res., Sect. A 365 (1995) 1–27.
[3] K. Aulenbacher, J. Schuler, D.V. Harrach, J. Appl. Phys. 92 (2002) 7536–7543.
[4] T. Maruyama, A. Brachmanna, J.E. Clendenin, *Phys. Rev.* A 492 (2002) 199–211.
[5] T. Siggins, C. Sinclair, C. Bohn, *Phys. Rev.* A 475 (2001) 549–553.
[6] A.A. Turnbull, G.B. Evans, J. Phys. D Appl. Phys. 1 (1968) 155.
[7] C.I. Wu, A. Kahn, J. Appl. Phys. 86 (1999) 3209–3212.
[8] Z.H. Chen, X.W. Jiang, S. Dong, et al., Appl. Phys. Lett. 104 (2014), 021120.
[9] Y. Shen, X.D. Yang, Y. Bian, S.M. Liu, K. Tang, R. Zhang, Y.D. Zheng, S.L. Gu, Mater. Res. Express 5 (2018), 015912.
[10] D.M. Ma, Y.F. Deng, D.P. Wang, et al., Superlattice. Microst. 128 (2019) 312–318.
[11] J.H. Jang, G. Cueva, D.C. Dumka, et al., Electron. Lett. 37 (2001) 707–708.
[12] C. Claeys, Y. Mols, et al., ECS J. Solid State Sci. Technol. 9 (2020), 033001.
[13] Z.G. Jia, Infrared Laser Eng. 6 (1999) 64–67 (in Chinese).
[14] D.G. Fisher, R.E. Enstrom, J. Appl. Phys. 43 (1972) 3815–3823.
[15] L. Zhao, Z.X. Guo, M. Zhang, et al., Surf. Interface Anal. 51 (2019) 498–505.
[16] J.P. Perdew, A. Zunger, Phys. Rev. B 23 (1981) 5048–5079.
[17] J.P. Perdew, K. Burke, M. Ernzerhof, Phys. Rev. Lett. 77 (1996) 3865–3868.

[18] T. Ohno, Surf. Sci. 357 (1996) 265–269.
[19] L.X. Zhang, W.E. McMahon, S.H. Wei, Appl. Phys. Lett. 96 (2010) 121912.
[20] H.P. Komsa, E. Arola, J. Pakarinen, S.P. Chang, T.T. Rantala, Phys. Rev. B 79 (2009) 115208.
[21] R.I. Eglitis, A.I. Popov, J. Saudi Chem. Soc. 22 (2018) 459–468.
[22] R.I. Eglitis, J. Purans, J. Gabrusenoks, A.I. Popov, R. Jia, Crystals 10 (2020) 745.
[23] N.D. Lang, W. Kohn, Phys. Rev. B 3 (1971) 1215–1223.
[24] L. Pauling, J. Am. Chem. Soc. 54 (1932) 3570–3582.
[25] M.B. Taylor, G.D. Barrera, N.L. Allan, T.H.K. Barron, Phys. Rev. B 56 (1997) 14380–14390.
[26] G.P. Srivastava, A.Z. AlZahrani, D. Usanmaz, Appl. Surf. Sci. 258 (2012) 8377–8386.
[27] Y.J. Du, B.K. Chang, X.H. Wang, J.J. Zhang, B. Li, M.S. Wang, Appl. Surf. Sci. 258 (2012) 7425–7428.
[28] G.G. Xu, Q.Y. Wu, J.M. Zhang, Z.G. Chen, Z.G. Huang, Acta Phys. Sin. 58 (2009) 1924–1930.
[29] X.H. Yu, Z.H. Ge, B.K. Chang, M.S. Wang, Mater. Sci. Semicond. Process. 16 (2013) 1813–1820.
[30] F.H. Wang, P. Krüger, J. Pollmann, *Phys. Rev*. B 64 (2001), 035305.
[31] R.I. Eglitis, Ferroelectrics 483 (2015) 53–67.
[32] W.E. Pickett, Comput. Phys. Rep. 9 (1989) 115–198.
[33] J. Guo, B.K. Chang, M.C. Jin, M.Z. Yang, H.G. Wang, M.S. Wang, Appl. Surf. Sci. 283 (2013) 954–957.
[34] X.H. Yu, J. Mater. Sci. 51 (2016) 8259–8269.
[35] O.Y. Khyzhun, et al., J. Mater. Sci. Mater. Electron. 27 (2016) 3258–3264.
[36] A.A. Lavrentyev, et al., Opt. Mater. 80 (2018) 12–21.
[37] P.W. Tasker, J. Phys. C Solid State Phys. 12 (1979) 4977–4984.
[38] Y.J. Du, B.K. Chang, H.G. Wang, J.J. Zhang, M.S. Wang, Chin. Optic Lett. 10 (2012), 051601.
[39] M. Arbi, N. Benramdane, Z. Kebbab, R. Miloua, F. Chiker, R. Khenata, Mater. Sci. Semicond. Process. 15 (2012) 301–307.